

A small payload desktop industry robot design without conventional reducers

Xiaolei Han¹, Peng Liu², Jiaqi Zhang²

¹Shanghai Business School, Shanghai, China

²Suzhou HULK Robot Company, Suzhou, China

Article Info

Article history:

Received Jun 29, 2023

Revised Dec 7, 2023

Accepted Dec 18, 2023

Keywords:

Desktop industry robot

Low cost

Small payload

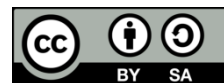
Synchronous belts

Without conventional reducers

ABSTRACT

Designing a compact desktop industrial robot with a small payload capacity, eliminating the use of traditional reducers, poses an intriguing challenge. This innovative approach aims to enhance the robot's cost-efficiency and reduce its overall size. The design focuses on optimizing the mechanical structure and exploring alternative mechanisms to achieve precise control without relying on conventional reducers. This article delves into the design aspects of a 1 kg payload robot. Initially, the paper presents an overview of the robot's mechanism and its kinematic analysis. Subsequently, synchronous belts are proposed as replacements for traditional reducers, accompanied by an introduction to the mechanical structure. Simulation is carried out to calculate the drive forces on the belts. According to the result, a suitable belt scheme has been designed. Ultimately, a prototype of the robot is constructed, and experiments demonstrate that this design achieves a repeatable accuracy comparable to robots employing conventional reducers, all while considerably reducing the overall cost of the robot.

This is an open access article under the [CC BY-SA](https://creativecommons.org/licenses/by-sa/4.0/) license.



Corresponding Author:

Jiaqi Zhang

Suzhou HULK Robot Company

Suzhou, Jiangsu, China

Email: zjq@hulkbot.com

1. INTRODUCTION

In the realm of robotics, the pursuit of compact and cost-effective designs has become a paramount consideration. This paper addresses the intriguing challenge of designing a small payload desktop industrial robot without resorting to conventional reducers. The conventional use of reducers has long been a standard in robot design, providing control and precision but often at the cost of increased size and expense. In response to this challenge, our innovative approach seeks to revolutionize the design paradigm by enhancing cost-efficiency and minimizing the overall footprint of the robot. The primary objective of this research is to explore alternative mechanisms that can effectively replace traditional reducers, focusing specifically on a compact desktop industrial robot with a small payload capacity. The elimination of conventional reducers not only poses an engineering challenge but also opens avenues for creating a more streamlined and economically viable robotic solution.

Multi-degree-of-freedom (DOF) robot arms designed for delicate movements are increasingly essential across various fields, including industry, service, and education. As the application of robots expands, there is a trend towards smaller robot sizes and payloads, allowing robots to work closely and even collaboratively with people. Notably, there has been significant development in the education sector, where small payload 6-DOF robot arms are designed to impart foundational knowledge of robotics and teach students how to program robots effectively [1]–[4]. Special kits enable students to construct their own robots

[5], [6], with an emphasis on simplicity rather than high accuracy and velocity. Steering engines and step motors typically suffice for joint driving in these educational contexts [7].

In contrast, research in the service robotics domain focuses on developing light and skillful arms, exploring ways to coordinate multiple arms to achieve specific tasks [8]–[11]. The emphasis in these cases is on efficient algorithms for robot control [12]–[14]. Another area of investigation is force control, covering contact force and self-weight compensation [15]–[17]. Researchers have designed specialized joint modules [18], [19] and dynamic algorithms to drive robot arms with active compensation torque. Some designs position motors at the base of the arm to prevent an increase in the robot arm's inertia, with power transmission achieved through wires and tubes.

In recent years, industrial applications have witnessed a growing frequency of operations involving payloads of 1 kg or less. However, industrial robots specifically designed for such small payload applications are relatively scarce. Examples include Yaskawa's 0.5 kg industrial robot called MotoMini and Nachi's 6-axis industrial robot named MZ01, boasting a 1 kg payload capacity. In China, small-payload robots are predominantly employed in education and training, such as the DOBOT series (0.5 kg payload) developed by Yuejiang and the TCR0.5/TCR1 desktop robots developed by Siasun. In industrial applications, most robot stations use higher payload robots to execute operations involving 1 kg and below. To strike a balance between cost reduction and maintaining performance in small payload applications, this article explores a novel design for a small payload robot.

Through a detailed kinematic analysis, we aim to elucidate the intricacies of the robot's mechanism, laying the foundation for subsequent discussions on the design innovations. The exploration of synchronous belts as a substitute for traditional reducers forms a central theme in our approach, offering a potential breakthrough in achieving precise control without the inherent drawbacks of conventional mechanisms.

As we progress through this study, a comprehensive examination of the robot's design principles, simulations, and experimental results will be presented. The ultimate goal is to demonstrate that our proposed design, tailored for a 1 kg payload robot, not only matches but surpasses the repeatable accuracy of robots equipped with traditional reducers. Moreover, we emphasize the noteworthy reduction in overall cost—a pivotal factor in advancing the feasibility and accessibility of such robotic solutions.

2. METHOD

2.1. Mechanism of the 1 kg payload robot

2.1.1. Mechanism determination

If a robot intends to execute tasks in a universal way, it necessitates a minimum of 6 degrees of freedom [20]–[22]. However, many applications only demand specific “degrees of freedom” actions to fulfill particular tasks, such as handling and placing objects within a horizontal plane [23]. In such instances, a reduced number of degrees of freedom, namely 3 or 4, proves sufficient. Taking into account considerations of both cost-effectiveness and practicality, the robot's mechanism is determined to have 4 degrees of freedom.

In industrial applications, two prevalent types of robots have found widespread use. The first is the SCARA robot, characterized by three rotational joints and one translational motion, as illustrated in Figure 1. However, in certain scenarios, there may be limitations in the vertical workspace. The second type is the palletizing industrial robot, depicted in Figure 2, featuring four rotating joints. Two sets of parallelogram mechanisms facilitate three-dimensional motion, ensuring the manipulator remains perpendicular to the ground. Notably, this configuration enables the placement of driving motors at the lower part of the robot. Throughout the robot's movement, the upper and forearm sections are relieved from bearing the weight of the motors. This aspect holds particular significance for a lightweight 1 kg robot. In conclusion, the palletizing robot mechanism proves to be more advantageous, offering enhanced maneuverability and alleviating the burden on the robot's structure during operation. The mechanism structure of the robot is shown in Figure 3, with L_1 representing the robot's waist, L_2 representing the robot's upper arm, and L_3 representing the robot's forearm [24].

2.1.2. Robot kinematics analysis

To facilitate the kinematic planning of the robot, it is imperative to establish the kinematic model, encompassing both forward and inverse kinematics [25]. The Denavit-Hartenberg (DH) coordinate system is established, as illustrated in Figure 4. The corresponding parameters are detailed in Table 1.

The process of determining the position and orientation of the end effector concerning the base coordinate, given the motor angular positions θ_1 , θ_2 , θ_3 and θ_4 , is referred to as forward kinematics. Utilizing the DH parameters of the robot, the coordinate transformation matrix from one joint to the next can be derived. Sequentially multiplying these coordinate transformation matrices yields the coordinate

transformation matrix from the base to the end effector. The respective coordinate transformation matrices are presented below:

$${}^1_0T = \begin{bmatrix} \cos\theta_1 & -\sin\theta_1 & 0 & 0 \\ \sin\theta_1 & \cos\theta_1 & 0 & 0 \\ 0 & 0 & 1 & 0 \\ 0 & 0 & 0 & 1 \end{bmatrix} \quad (1)$$

$${}^2_1T = \begin{bmatrix} \cos\theta_2 & -\sin\theta_2 & 0 & a_1 \\ 0 & 0 & 1 & B_1 \\ -\sin\theta_2 & -\cos\theta_2 & 0 & 0 \\ 0 & 0 & 0 & 1 \end{bmatrix} \quad (2)$$

$${}^3_2T = \begin{bmatrix} \cos\theta_3 & -\sin\theta_3 & 0 & a_2 \\ \sin\theta_3 & \cos\theta_3 & 0 & 0 \\ 0 & 0 & 1 & 0 \\ 0 & 0 & 0 & 1 \end{bmatrix} \quad (3)$$

$${}^4_3T = \begin{bmatrix} \cos\theta_4 & -\sin\theta_4 & 0 & a_3 \\ \sin\theta_4 & \cos\theta_4 & 0 & 0 \\ 0 & 0 & 1 & 0 \\ 0 & 0 & 0 & 1 \end{bmatrix} \quad (4)$$

$${}^5_4T = \begin{bmatrix} \cos\theta_5 & -\sin\theta_5 & 0 & a_4 \\ 0 & 0 & -1 & B_2 \\ -\sin\theta_5 & -\cos\theta_5 & 0 & 0 \\ 0 & 0 & 0 & 1 \end{bmatrix} \quad (5)$$

$${}^5_0T = {}^1_0T {}^2_1T {}^3_2T {}^4_3T {}^5_4T = \begin{bmatrix} \cos\theta_1 \cos\theta_5 - \sin\theta_1 \sin\theta_5 & -\cos\theta_1 \sin\theta_5 - \sin\theta_1 \cos\theta_5 & 0 & p_x \\ \sin\theta_1 \cos\theta_5 + \cos\theta_1 \sin\theta_5 & -\sin\theta_1 \sin\theta_5 - \cos\theta_1 \cos\theta_5 & 0 & p_y \\ 0 & 0 & -1 & p_z \\ 0 & 0 & 0 & 1 \end{bmatrix} \quad (6)$$

where:

$$p_x = \cos\theta_1(A_1 + A_3 \cos\theta_{23} + A_2 \cos\theta_2 + A_4)$$

$$p_y = \sin\theta_1(A_1 + A_3 \cos\theta_{23} + A_2 \cos\theta_2 + A_4)$$

$$p_z = B_1 - B_2 - (A_3 \sin\theta_{23} + A_2 \sin\theta_2)$$

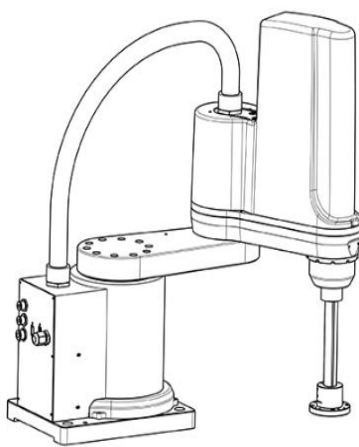


Figure 1. SCARA robots

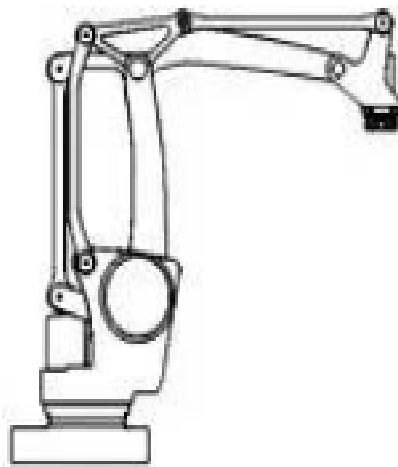


Figure 2. Palletizing robot

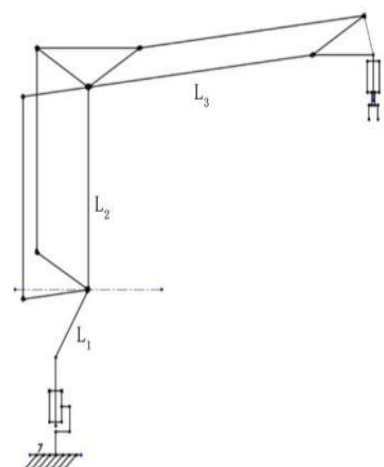


Figure 3. The mechanism structure of the robot

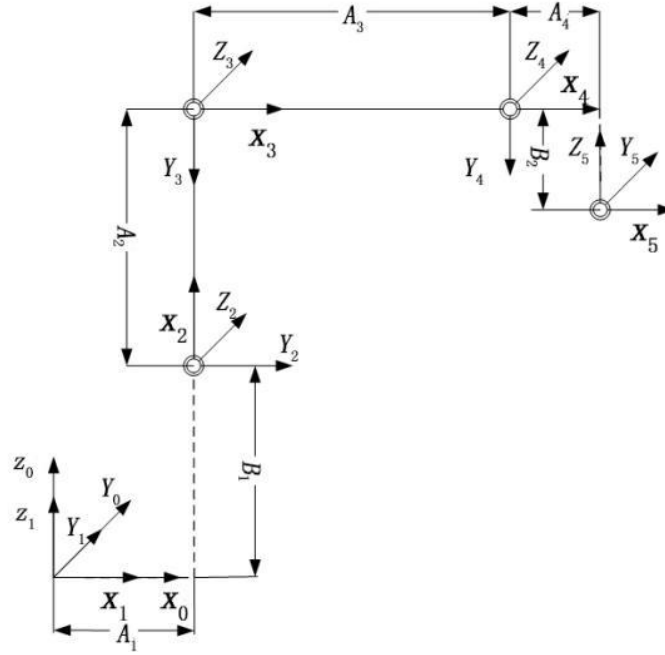


Figure 4. The D-H coordinate system

Table 1. Parameters of the DH coordinate system

Link no.	A_{i-1}	A_{i-1}	D_i	θ_i	Range of the joints
1	0	0	0	θ_1	$-170^\circ \sim 170^\circ$
2	A_1	-90°	B_1	θ_2	$-145^\circ \sim 0^\circ$
3	A_2	0	0	θ_3	$\theta_1 \leq \theta_3 \leq \theta_k$
4	A_3	0	0	θ_4	$-\theta_2 \sim \theta_3$
5	A_4	90°	$-B_2$	θ_5	$-165^\circ \sim 165^\circ$

When the position and orientation of the end effector are given in relation to the robot base coordinate, determining the angular positions of the joints $\theta_1, \theta_2, \theta_3, \theta_4$ is termed the inverse kinematics of the robot. In the context of a serial mechanism, notable methods for solving inverse kinematics encompass the algebraic solution and the geometric solution. The algebraic solution method tends to be more computationally intensive. However, given the straightforwardness of the robot model, the geometric solution proves advantageous in significantly reducing trajectory planning time. Referring to (7),

$${}^1T^{-1}{}^4T = {}^1T^{-1}{}^1T_2{}^1T_3{}^1T_4T = {}^1T \quad (7)$$

θ_1 can be solved:

$$\theta_1 = \arctan2(p_x, p_y) \quad (8)$$

By substituting it into (6), θ_3 and θ_5 are obtained, where

$$\theta_3 = \arccos\left(\frac{p_x^2 + p_y^2 + p_z^2 - 2A_1(\cos\theta_1 p_x + \sin\theta_1 p_y) + A_1^2}{2A_2A_3}\right) \quad (9)$$

$$\theta_5 = \arctan2({}^5T_{21}\cos\theta_1 - {}^5T_{11}\sin\theta_1, {}^5T_{11}\cos\theta_1 + {}^5T_{21}\sin\theta_1) \quad (10)$$

By substituting θ_3 and θ_5 into the (11):

$${}^3T^{-1}{}^4T = {}^3T \quad (11)$$

obtains:

$$\theta_{23} = \arctan2[-(A_3 + A_2 \cos \theta_3)p_z - A_2 \sin \theta_3(p_x \cos \theta_1 + p_y \sin \theta_1 - A_1), (A_3 + A_2 \cos \theta_3)(p_x \cos \theta_1 + p_y \sin \theta_1 - A_1) - A_2 p_z \sin \theta_3] \quad (12)$$

θ_2 and θ_4 can be calculated according to (13) and (14).

$$\theta_2 = \theta_{23} - \theta_3 \quad (13)$$

$$\theta_4 = -\theta_2 - \theta_3 \quad (14)$$

2.1.3. Mechanism parameters design

The optimized mechanism parameters are $A_1=30.5$ mm, $A_2=240$ mm, $A_3=260$ mm, $A_4=55$ mm, $B_1=278.5$ mm, $B_2=50$ mm. Due to the limitation of the parallelogram structure, θ_3 is relevant to θ_2 and its ranges are given as (15):

$$\begin{cases} -\theta_2 - 25^\circ \leq \theta_3 \leq 160^\circ & (-135^\circ \leq \theta_2 < -107^\circ) \\ 58^\circ \leq \theta_3 \leq 160^\circ & (-107^\circ \leq \theta_2 < -53^\circ) \\ 58^\circ \leq \theta_3 \leq -\theta_2 + 106^\circ & (-53^\circ \leq \theta_2 \leq 0^\circ) \end{cases} \quad (15)$$

2.1.4. 3D model of the robot arm

The mechanical structure of the robot is designed, as depicted in Figure 5. The robot comprises a base, a controller box, a driving motor cabinet, an upper arm, and a forearm. To achieve weight reduction, the majority of the robot parts are constructed from aluminum alloy. The structures are optimized for increased compactness and reliability. Additionally, a controller board and motor drivers are designed in-house, with all electrical and electronic components housed within the controller box and the base. This compact design eliminates the need for an extra electrical cabinet.

Reducers play a pivotal role in the functionality of industrial robots. RV reducers are commonly employed in applications with high payload and precision, while harmonic reducers find application in scenarios with high precision and medium payload. Regardless of the type chosen, reducers tend to incur relatively high costs, particularly for robots with a payload of 1 kg and below. Given the lower popularity and quantity of such smaller robots compared to their larger counterparts, reducers become less economically viable. In light of this, there is a necessity to devise a suitable reduction unit that balances considerations of stability, transmission accuracy, and cost-effectiveness. Two-stage synchronous belt reducers are designed to achieve speed reduction.

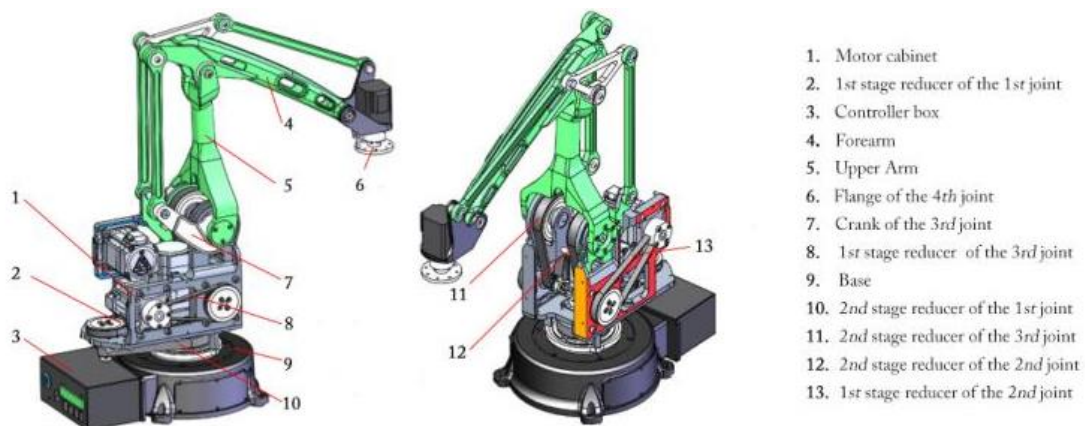


Figure 5. The 3D model of the 1 kg payload robot

2.1.5. Simulations of the robot arm

In the following simulations, the kinematic model and the robot's workspace is analyzed [26]. By using the forward kinematic discussed above, the set of the end effector positions $[p_x, p_y, p_z]$ can be solved.

The boundary points of the end effector can be chosen to visualize the workspace which are shown in Figure 6.

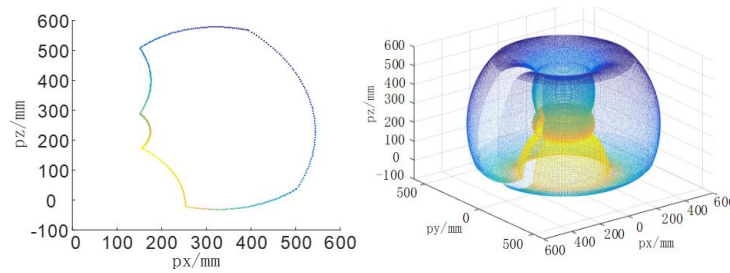


Figure 6. Workspace of the end effector

The closed curve on the left in Figure 6 shows the boundary of the robot's workspace on the XZ plane when θ_1 is zero, the area enclosed within the boundary represents the robot's operational plane. As this area rotates around the Z-axis from -170° to 170° , the entire three-dimensional workspace of the robot is depicted in the right picture of Figure 6. According to this working space, the position of the robot in the assembling line can be decided to maximize efficiency.

2.2. Dynamics of the 1 kg payload robot

Considering the actual working range and motion states of the robot, when the robotic arm is extended to its furthest point under a loaded condition, the first axis of the robot needs to bear the rotational inertia generated by the entire movable component rotating around the first axis to maintain a high dynamic response. This posture represents the most adverse force scenario for the robot. The forces experienced by the transmission components of the robot's first axis will reach the maximum within the entire workspace. This force serves as the input criterion for selecting and calculating the belt transmission for the robot's first, second, and third axes.

2.2.1. Simulation of drive forces in extreme robot pose

The first joint is driven by a motor with a two-stage synchronous belt reducer, enabling vertical rotation. Similarly, the second and third joints are driven by motors with two-stage synchronous belt reducers, facilitating rotations of the upper arm and forearm. The fourth axis, situated at the end of the forearm, is directly driven by a motor for rotation. The first three motors and their reducers are housed in the driving motor cabinet above the base to minimize the mass and moment of inertia of the robot arm. This design reduces unnecessary payload on the motors, enhancing the response speed of the robot arm.

Initially, the robot undergoes model processing, establishing a simulation model imported into SolidWorks. The robot's end effector is loaded with 1 kg, and the robot's arm is extended to its maximum as shown in Figure 7. This model is used to simulate the dynamic output changes of the robot's first axis in extreme poses. The mechanical design of the belt transmission for the first axis is shown in Figure 8.

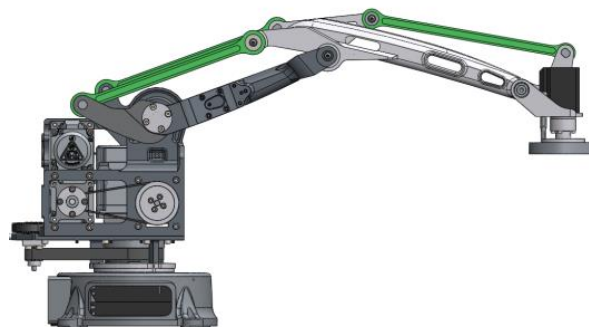


Figure 7. Robot in extreme pose

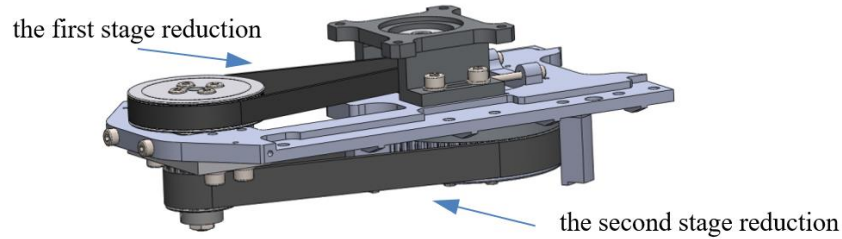


Figure 8. The mechanical design of the belt transmission for the first axis

Next, velocity and trajectory planning are required for the first axis, as shown in Figure 9. The red curve represents the velocity profile, with a maximum speed of $180^\circ/\text{s}$, while the blue curve represents the displacement profile. Subsequently, based on SolidWorks dynamic simulation, the output torque variation of the deceleration components for the first axis can be computed, as illustrated in Figure 10.

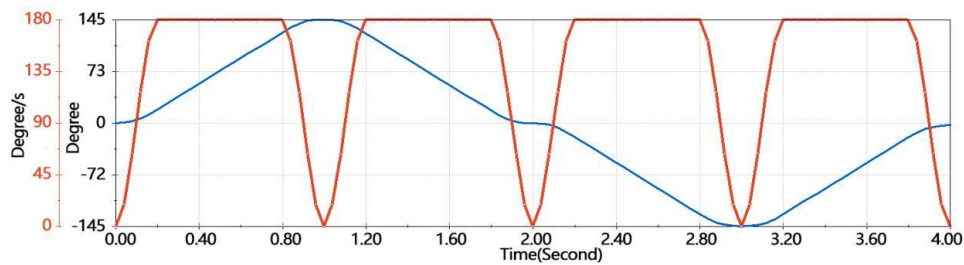


Figure 9. Velocity and trajectory planning of the first axis

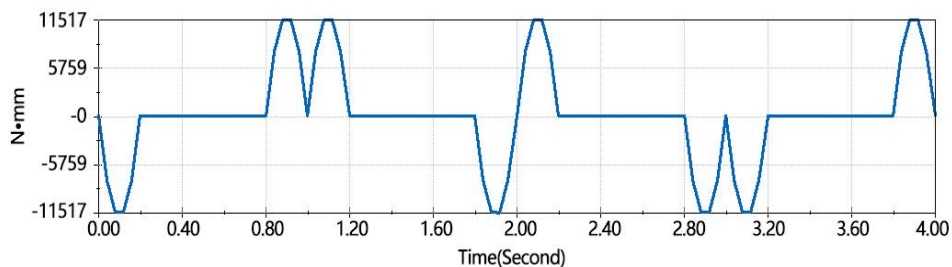


Figure 10. The torque variation of the first axis

2.2.2. Selection of belt transmission parameters

Finally, based on the above dynamic simulation results, the maximum output torque for the first axis of the robot is determined to be 11.5 Nm. This value is used as the input torque for belt selection. Considering the reduction ratio of the two-stage reducer and the dimensions of the robot body, the number of teeth for the two-stage reduction pulleys for the first axis is determined as follows:

For the first stage reduction synchronous pulleys of the first axis:

- Small pulley: 16 teeth
- Large pulley: 48 teeth

For the second stage reduction synchronous pulleys of the first axis:

- Small pulley: 14 teeth
- Large pulley: 48 teeth

Furthermore, based on the operating conditions, center distance adjustment range, and pulley teeth, it is straightforward to determine the width of the synchronous belt and pulley. For interchangeability, it is advisable to keep the pulleys for the second and third axes of the robot as consistent as possible with the first axis. Consequently, the first three joints of the robot employ a two-stage synchronous belt reducer. The reduction ratios for these joints are detailed in Table 2, while the fourth joint of the robot is driven by a motor without a reducer.

Table 2. The reduction ratios of the first three joints

No. of joint	No. of stage	Ratio of single stage	Reduction Ratio
1 st joint	1 st	1 : 3.33333	1: 11.42857
	2 nd	1 : 3.42857	
2 nd joint	1 st	1 : 3.33333	1 : 10.47619
	2 nd	1 : 3.14286	
3 rd joint	1 st	1 : 3.33333	1 : 10.47619
	2 nd	1 : 3.14286	

3. RESULTS AND DISCUSSION

Based on the structural parameters, a prototype of the robot is manufactured. To assess reposition accuracy, a dedicated test environment is created, as depicted in Figure 11. During testing, the robot's end effector moves from various positions to the same point, with a dial test indicator recording the error on each occasion. The image on the right displays the error data from 1,000 motion tests. It is evident that the repeatable position accuracy of the robot falls within ± 0.05 mm, reaching the typical standard of industrial robots equipped with conventional RV or harmonic reducers.

Subsequently, this production has been introduced to the market, primarily finding applications in the 3C and auto parts sectors. For instance, the robot is employed in tasks such as transporting smartphones for laser engraving and assembling auto engines, as illustrated in Figure 12.

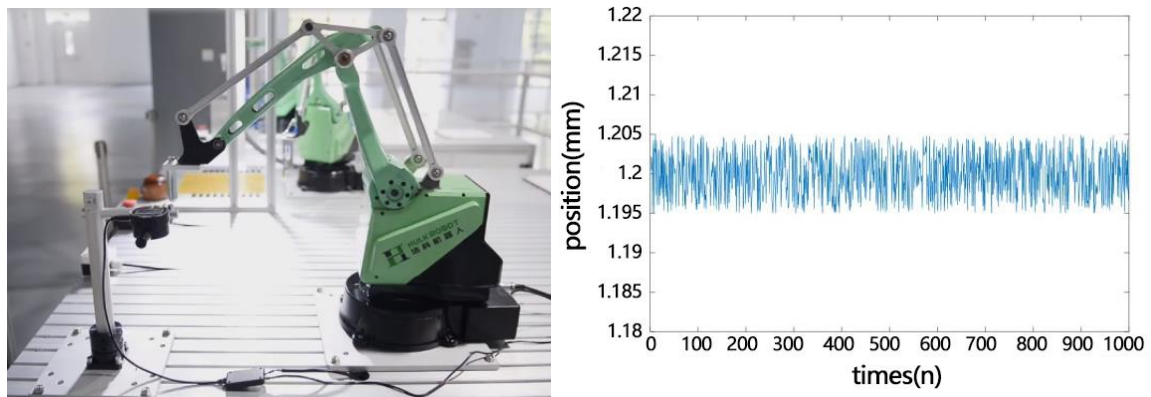


Figure 11. The test of the prototype for the repeatable position accuracy



Figure 12. Industrial application cases

4. CONCLUSION

In response to specific application requirements, a 4-DOF desktop industrial robot has been meticulously designed. The determination of the mechanism and subsequent establishment of kinematic models were the initial steps. An analysis of the robot's workspace was conducted, followed by the introduction of the synchronous belt transmission method to address stability, transmission accuracy, and cost-effectiveness needs. The mechanical structure was then designed accordingly.

Subsequently, the robot prototype underwent testing to validate its repeatable position accuracy. The results demonstrate that the repeatability of this robot matches that of counterparts equipped with RV and harmonic reducers, while maintaining significantly lower costs. Therefore, for small payload desktop industrial applications, the design presented in this paper offers a distinct advantage.

ACKNOWLEDGEMENTS

This paper is supported by Jiangsu Key Research and Development Project (BE2020101) and Suzhou Key Research and Development Project (SGC2021069).

REFERENCES





- [1] A. M. Cook, B. Bentz, N. Harbottle, C. Lynch, and B. Miller, "School-based use of a robotic arm system by children with disabilities," *IEEE Transactions on Neural Systems and Rehabilitation Engineering*, vol. 13, no. 4, pp. 452–460, Dec. 2005, doi: 10.1109/tnsre.2005.856075.
- [2] R. A. Bindu, S. Alam, and A. A. Neloy, "A cost-efficient multipurpose service robot using Raspberry Pi and 6 DOF robotic arm," in *Proceedings of the 2019 2nd International Conference on Service Robotics Technologies*, Mar. 2019, doi: 10.1145/3325693.3325701.
- [3] R. Siemasz, K. Tomczuk, and Z. Malecha, "3D printed robotic arm with elements of artificial intelligence," *Procedia Computer Science*, vol. 176, pp. 3741–3750, 2020, doi: 10.1016/j.procs.2020.09.013.
- [4] D. R. Vyas, A. Markana, and N. Padhiyar, "Economic 6-DOF robotic manipulator hardware design for research and education," *Materials Today: Proceedings*, vol. 62, pp. 7179–7184, 2022, doi: 10.1016/j.matpr.2022.03.140.
- [5] Y. Mitabe, N. Sathyakumar, C. G. Parthiban, S. Rajaganapathi, and S. R. Pandian, "A build your own robot manipulator for manufacturing education," in *2017 6th International Conference on Computer Applications In Electrical Engineering-Recent Advances (CERA)*, Oct. 2017, doi: 10.1109/cera.2017.8343381.
- [6] F. Ghadamli and B. Linke, "Development of a desktop hybrid multipurpose grinding and 3D printing machine for educational purposes," *Procedia Manufacturing*, vol. 5, pp. 1143–1153, 2016, doi: 10.1016/j.promfg.2016.08.090.
- [7] J. Silva, P. Costa, and J. Goncalves, "Description of a new servo motor optimized for educational robotic applications," in *2018 13th APCA International Conference on Control and Soft Computing (CONTROL)*, Jun. 2018, doi: 10.1109/control.2018.8514287.
- [8] A. Rodić, B. Miloradović, S. Popić, and Đ. Urukalo, "On developing lightweight robot-arm of anthropomorphic characteristics," in *Mechanisms and Machine Science*, Springer International Publishing, 2015, pp. 33–46.
- [9] G. R. B. E. Romer, H. J. A. Stuyt, and A. Peters, "Cost-savings and economic benefits due to the assistive robotic manipulator (ARM)," in *9th International Conference on Rehabilitation Robotics*, pp. 201–204, doi: 10.1109/ICORR.2005.1501084.
- [10] R. M. Alqasemi, E. J. McCaffrey, K. D. Edwards, and R. V. Dubey, "Analysis, evaluation and development of wheelchair-mounted robotic arm," in *9th International Conference on Rehabilitation Robotics*, doi: 10.1109/icorr.2005.1501144.
- [11] H.-S. Kim and J.-B. Song, "Multi-DOF counterbalance mechanism for a service robot arm," *IEEE/ASME Transactions on Mechatronics*, vol. 19, no. 6, pp. 1756–1763, Dec. 2014, doi: 10.1109/tmech.2014.2308312.
- [12] E.-J. Kim, K. Seki, and M. Iwasaki, "Motion control of industrial robots by considering serial two-link robot arm model with joint nonlinearities," *Journal of Mechanical Science and Technology*, vol. 28, no. 4, pp. 1519–1527, Apr. 2014, doi: 10.1007/s12206-014-0139-x.
- [13] Q. Ai, Q. Yang, M. Li, X. Feng, and W. Meng, "Implementing multi-DOF trajectory tracking control system for robotic arm experimental platform," in *2018 10th International Conference on Measuring Technology and Mechatronics Automation (ICMTMA)*, Feb. 2018, doi: 10.1109/icmtma.2018.00075.
- [14] C. Li, X. Chen, X. Ma, H. Sun, and B. Wang, "Skill acquisition and controller design of desktop robot manipulator based on audio-visual information fusion," *Machines*, vol. 10, no. 9, Sep. 2022, doi: 10.3390/machines10090772.
- [15] H. Jamshidifar *et al.*, "A novel mechanism for gravity-balancing of serial robots with high-dexterity applications," *IEEE Transactions on Medical Robotics and Bionics*, vol. 3, no. 3, pp. 750–761, Aug. 2021, doi: 10.1109/tmrb.2021.3098124.
- [16] M. Sato and S. Katsura, "Active self-weight compensation for direct-drive robot arm," in *IECON 2022 – 48th Annual Conference of the IEEE Industrial Electronics Society*, Oct. 2022, doi: 10.1109/iecon49645.2022.9968990.
- [17] H. Huang, E. Dong, L. Zhou, M. Xu, and J. Yang, "Design and analysis of a bionic two-DOF joint for dual-arm manipulator," in *2016 IEEE International Conference on Robotics and Biomimetics (ROBIO)*, Dec. 2016, doi: 10.1109/robio.2016.7866487.
- [18] H.-S. Kim *et al.*, "Advanced 2-DOF counterbalance mechanism based on gear units and springs to minimize required torques of robot arm," *IEEE Robotics and Automation Letters*, vol. 7, no. 3, pp. 6320–6326, Jul. 2022, doi: 10.1109/lra.2022.3168936.
- [19] I. Daniyan, K. Mpofu, B. Ramatsetse, and A. Adeodu, "Design and simulation of a robotic arm for manufacturing operations in the railcar industry," *Procedia Manufacturing*, vol. 51, pp. 67–72, 2020, doi: 10.1016/j.promfg.2020.10.011.
- [20] L. Fiorio, A. Scalzo, L. Natale, G. Metta, and A. Parmiggiani, "A parallel kinematic mechanism for the torso of a humanoid robot: Design, construction and validation," Sep. 2017, doi: 10.1109/iros.2017.8202225.
- [21] B. Hu *et al.*, "Reachable workspace determination for a spatial hyper-redundant manipulator formed by several parallel manipulators," *Journal of Mechanical Science and Technology*, vol. 33, no. 2, pp. 869–877, Feb. 2019, doi: 10.1007/s12206-019-0144-1.
- [22] T. T. Tung, N. Van Tinh, D. T. Phuong Thao, and T. V. Minh, "Development of a prototype 6 degree of freedom robot arm," *Results in Engineering*, vol. 18, Jun. 2023, doi: 10.1016/j.rineng.2023.101049.
- [23] E. A. Rubleva and A. B. Mudrich, "Kinematic model of a desktop robot manipulator with 5 degrees of freedom," *Journal of*

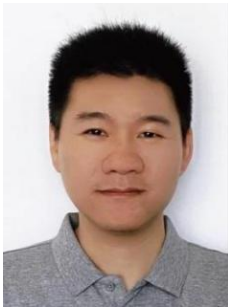
Physics: Conference Series, vol. 2096, no. 1, p. 12178, Nov. 2021, doi: 10.1088/1742-6596/2096/1/012178.





- [24] S. Briot and A. Goldsztejn, "Topology optimization of industrial robots: application to a five-bar mechanism," *Mechanism and Machine Theory*, vol. 120, pp. 30–56, Feb. 2018, doi: 10.1016/j.mechmachtheory.2017.09.011.
- [25] R. P. Paul and C. N. Stevenson, "Kinematics of robot wrists," *The International Journal of Robotics Research*, vol. 2, no. 1, pp. 31–38, Mar. 1983, doi: 10.1177/027836498300200103.
- [26] G. Yang, W. Lin, S. Mustafa, I. Chen, and S. Yeo, "Numerical orientation workspace analysis with different parameterization methods," Dec. 2006, doi: 10.1109/ramech.2006.252717.

BIORAPHS OF AUTHORS







Xiaolei Han     is a lecturer in IoT Engineering of Shanghai Business School. She got his Ph.D. from Tongji University and she did her post-doc research at Shanghai Jiao Tong University. Her master's major was signal and information processing, and her doctor's major was control theory and control engineering. Her main research directions include artificial intelligence algorithms, embedded system design, and computer vision. She can be contacted at hanxl@sbs.edu.cn.



Peng Liu     is a senior engineer of Suzhou HULK Robot Company. He got his master's degree from Yanshan University and majored in mechanical engineering. He has more than 10 years experience in designing robot mechanism. He can be contacted at lp@hulkbot.com.



Jiaqi Zhang     is the CEO of Suzhou HULK Robot Company. He got his PhD from Tongji University and finished his post-doc research at Shanghai Jiao Tong University. He was a visiting student in UC Berkeley during his PhD period. His research focus on robot control. He can be contacted at email: zjq@hulkbot.com.